Hindawi Publishing Corporation
EURASIP Journal on Wireless Communications and Networking
Volume 2009, Article ID 618036, 13 pages
doi:10.1155/2009/618036

Research Article

Experimental Data Collection and Performance Analysis of Outdoor UWB Positioning System under Static and Mobile Conditions

Paul Richardson and Dan Shan

Department of Electrical and Computer Engineering, University of Michigan-Dearborn, 4901 Evergreen Road., Dearborn, MI 48128, USA

Correspondence should be addressed to Paul Richardson, richarpc@umich.edu

Received 16 August 2009; Revised 3 December 2009; Accepted 15 December 2009

Recommended by Weidong Xiang

A wide variety of semiautonomous systems are emerging in construction, defense, and agricultural applications. A UWB positioning system shows promise in improving navigational capabilities and safety of operations for these systems. This paper describes an outdoor UWB positioning system used to measure the position of the operators of a semiautonomous vehicle to improve safety of operations. A measurement campaign was conducted to collect experimental range errors for the system at distances from 2 m to 40 m. The range errors are characterized and performance of the system is assessed in a static environment. A model is proposed for range errors and results are compared to experimental data. Measured position errors are compared to position errors generated by the model. A mobility model is proposed and performance of the positioning system in a mobile environment is assessed.

1. Introduction

Ultra-wideband Impulse Radio (UWB-IR) systems are able to achieve fine time resolution using very narrow pulses. Accurate time measurements yield accurate range measurements that provide a building block for positioning systems, a capability emerging in a diverse range of applications [1–5]. In this effort we present an analysis of range and position measurement accuracy based on experimental data for a UWB-IR positioning system developed for outdoor environments. Outdoor UWB positioning systems provide an important capability for emerging semiautonomous applications in defense, construction, and agricultural vehicles. Accurate position measurements with high update rates can be used to enhance navigation, especially in GPS denied environments such as deep canyons and heavily forested terrain. Positioning data can improve safety of operations by providing operators and vehicle control systems with position information of nearby objects. This data can also facilitate certain autonomous applications such as "leader-follower" wherein a trailing vehicle will automatically follow a designated operator or vehicle.

The UWB positioning system was developed as a component of a semiautonomous control system hosted on a John Deere R-Gator, shown in Figure 1. The UWB positioning system consists of a four UWB radio range sensors, one mounted on each corner of the vehicle and a controller. The range sensors are used to measure range to a target and the data is passed to the controller via an Ethernet connection. The controller manages the system which includes calculation of target position, determination of which sensors are used to range to a target, and other management functions. A detailed description of the UWB sensors and system operation is provided in Section 2.

The overall effort was supported by the U.S. Department of Defense (DoD) with the objective of developing a medium-sized semiautonomous platform with "leader follower" capability. The UWB system measures the position of up to five operators around the platform and passes the data to the vehicle's control system. The vehicle control

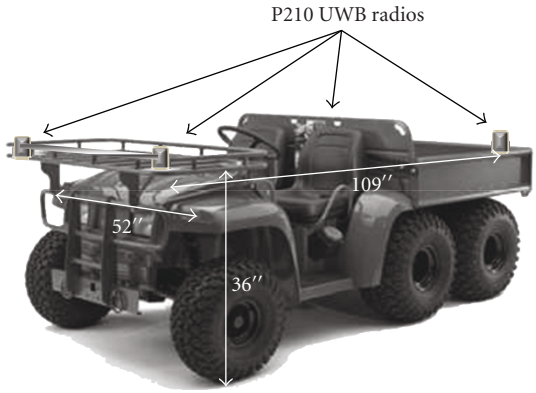

Figure 1: Position of UWB radios and dimensions of an R-Gator that hosted UWB positioning system.

system uses the data to dynamically determine a path to follow a designated operator and to avoid hitting others. The system has a separate radar system for obstacle detection. For safety reasons, limited speed zones are established (see Table 1) for maximum relative platform speeds around operators to compensate for position measurement errors, control error, and vehicle inertia. Vehicle speed beyond 20 meters is primarily limited by terrain conditions and top vehicle speed is 8.8 m/s.

The UWB positioning system uses commercially available programmable UWB radios and achieves accurate positioning at distances up to 40 meters with 20–25 Hz update rate for each position measurement. The UWB radios are programmed and calibrated to optimize for high update rate and accurate range measurements in an unobstructed path. An integrated controller collects range data, calculates position measurements, and controls the system's steering, braking, throttle, and transmission. The system provides 360° coverage for up to five operators at distances between two and forty meters from the vehicle's center. This information is used to improve safety by limiting vehicle speeds based on proximity to operators. The main focus of this effort is the analysis of UWB range errors and update rate based on an experimental data collection and the ensuing impact on position measurements in static and mobile conditions. In this initial phase, we analyze performance in a flat open grassy field and in an urban environment at distances up to forty meters. Future phases will address more complex channel environments such as hilly terrain and obstructed channels.

1.1. Previous Related Work. Increasing interest is shown towards UWB positioning and tracking systems [1–5]. The main focus of such systems has been for indoor environments, with scant data available for outdoor systems at longer ranges. UWB tracking has been explored for space applications [1, 2], commercial asset tracking [3, 4], and assistance to disabled persons [5]. Mahfouz et al. [6] describe a UWB indoor local positioning system that uses a 300 ps Gaussian pulse modulated on an 8 GHz carrier to provide accurate

Table 1: Safety limitation for platform speeds near operators.

distance from nearest operator less than 2 meters	maximum platform speed 0 m/s
2–5 meters	1.10 meters/second
5–10 meters	2.20 meters/second
10–15 meters	3.30 meters/second
15–20 meters	4.40 meters/second

range measurements at short ranges in an indoor environment. The author analyzes errors caused by multipath interference, sampling rate limitations, tag synchronization, and antenna phase variations. Experimental data is presented and a path to achieve very high accuracy in an indoor environment is described. In [7] a report of an indoor range measurement experiment using UWB IR radio is presented for LOS and NLOS intraroom propagation conditions.

Several projects [8–17] have addressed important issues regarding position estimation techniques. In [8] position estimates based on TOA signals are presented using classical filtering and an alternate approach that does not require knowledge of range error distribution. A novel joint position estimation approach using time-of-arrival (TOA) and direction-of-arrival (DOA) integrated with an extended Kalman Filter is proposed in [9] to achieve robust positioning. In [10], analysis of TOA-based estimation mechanisms is provided that addresses design of receiver architectures for UWB systems and provides simulation of the architectures using the 802.15.4a channel model. In [11], the authors propose an adaptive combining approach to reduce position measurement uncertainty. The approach combines TDOA measurements and uses directional motion increments to reduce random channel noise and dilution of precision (DOP). The approach shows promise to improve performance over existing methods because of its low cost and battery life impacts. NLOS channels are studies in [12–15]. In [12], the authors address challenges for indoor NLOS channels using a hybrid TDOA/AOA positioning approach. An analysis using modified extended Kalman Filter (MEKF) & modified regularized particle filter (MRPF) for position estimation in a mobile indoor environment is provided in [13]. In [15] the authors propose the use of RMS delay spread to detect NLOS propagation conditions which enables effective use of algorithms developed to alleviate NLOS propagation affects. In [16] the authors evaluate the performance of particle filters to improve raw position errors for a hybrid GPS-UWB system to track vehicles on the highway and in warehouses. The GPS is used for tracking outdoors and a UWB system is used to track within warehouses. In [17] the authors evaluate the range error of a pulsed UWB system, concluding that accuracy at longer distance depends on pulse spectrum and that short transmit pulses are necessary in dense multipath environment to maintain accuracy.

This effort presents experimental data for an outdoor, long range UWB positioning systems that have not previously been reported in the literature. We present the

accuracy of range measurements based on experimental data collection and the ensuing impact on position measurements in static and mobile environments. A model based on Gaussian distribution of range errors is proposed and compared to experimental results. The fundamental tradeoff between range accuracy and range update delay in a mobile environment is discussed and simulation results are presented. Estimation and prediction are core issues for improving positioning and tracking performance that are also related to the mobility model of the system. The detailed discussion of these issues and the study of more complex channel environments are beyond the scope of this paper and will be the subject of studies in the near future.

In the next section, an overview of the UWB radios and tracking system is provided. Section 3 presents the characteristics of the range measurement error based on experimental data collection and discusses the impact on position measurement error in a static environment. Section 4 presents a mobility model and assesses the impact of target motion on position measurement errors. Section 5 provides a summary and identifies areas of future work.

2. System Overview

This section provides an overview of the UWB positioning system from the perspective of understanding the characteristics of the errors and delays in measuring range and their affect on position measurements in static and mobile environments.

2.1. UWB Radio Description. The system uses the P210 radio from Time Domain, a time hopping, UWB-IR with capability for extended range measurements in outdoor environments. The radio transmits a pulse train with a 9.6 MHz pulse rate and time hop code of length 16. The pulse width at the internal SRD diode is 0.235 nanosecond and has a center frequency of f_c = 4.26 GHz. The pulse is high pass filtered in order to conform to the FCC mask for UWB at 3.1 GHz. Measured 10 dB frequency response of the radio is from 3.1 GHz to 5.8 Ghz. The radio can operate as a conventional radio transmitting data packets or it can send special 1/2 duplex range packets that measure time delay between any two radios. Higher layer services for data link control or networking must be provided by the user. The radio supports a 40 MHz Strong Arm Processor with 32 MB RAM and an Ethernet 10BaseT interface to host higher level services or user applications. The radio has a wide range of parameter settings that provide flexibility for making tradeoffs such as transmission delay versus reliability and range update rate versus range accuracy. A description of tradeoffs for several important parameters is provided in Section 3.

The P210 data packet consists of a synchronization preamble and payload data segment. Additional segments to support upper layer services (e.g., MAC or Network) can be added to the payload segment by the user. The parameter settings for synchronization affect the tradeoff between packet loss rate, maximum distance, and transmission delay. The primary parameters for synchronization include pulse integration, correlator sampling interval, and threshold settings. During packet synchronization, the radios have I-Q correlator pairs that sample at the time hop intervals. The correlator outputs are integrated and compared to a threshold that detects acquisition. The correlator sampling interval is adjustable and has a default step size of 235 ps or approximately one pulse width. The symbol energy, E_s, can be increased during synchronization using a pulse integration process, wherein the number of pulses that represent a synchronization symbol is increased as a power of two from 2^4 to 2^{10}. Each increment in pulse integration doubles the accumulated signal voltage, providing a 6 dB increase in signal power. Gaussian noise increases by a factor of 1.41 dB for a 3 dB increase in power. Thus each doubling of integration yields approximately 3 dB increase in signal-to-noise ratio (SNR). However, increasing integration also increases the transmission delay. The number of synchronization symbols is adjustable and the default value is 443 symbols, which allows the correlators to sample (step) over one pulse interval of 104 nanoseconds searching for a valid preamble as shown in (1),

$$\frac{T_{\text{pulse}}}{T_{\text{sample}}} = \frac{104\,\text{ns}}{235\,\text{ps}} = 443 \text{ symbols}, \tag{1}$$

where T_{pulse} is the pulse period and T_{sample} is the correlator sampling period. The transmission delay for the synchronization preamble is given by

$$\frac{I \times N_s}{R_{\text{pulse}}}, \tag{2}$$

where I is the synchronization integration, N_s is the number of synchronization symbols, and R_{pulse} is the pulse rate. The receiver threshold can be set either manually or automatically. The automatic mode adds an additional $N_s/2$ symbols to the synchronization preamble. The correlator outputs over the initial $N_s/2$ symbols are used to estimate SNR and the synchronization threshold is set based on the estimated SNR. Autothresholding is effective in a dynamic channel environment but increases synchronization delay by 50%. The various methods to reduce packet error rate (e.g., increasing I, reducing T_{sample}, automatic thresholding) and the accompanying increase in transmission delay defines one of the key tradeoffs in mobile positioning accuracy that must be carefully studied.

2.2. Range Packets and Measuring Range. The range between two radios is determined by measuring the round trip propagation delay via the exchange of special "request" and "response" packets. While this takes longer than simplex ranging systems, it has the benefit that it does not require central clock synchronization. Measuring range includes an initial coarse measurement and a fine adjustment step known as leading edge detection (LED). In the initial step (Figure 2) the requester time stamps the transmit time of a range request at ts_1 and then transmits the packet. The responder time stamps the arrival of the range request at ts_2, performs

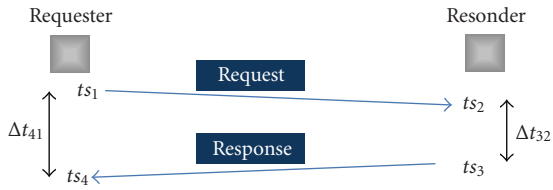

Figure 2: Half Duplex range packets used to measure coarse propagation delay.

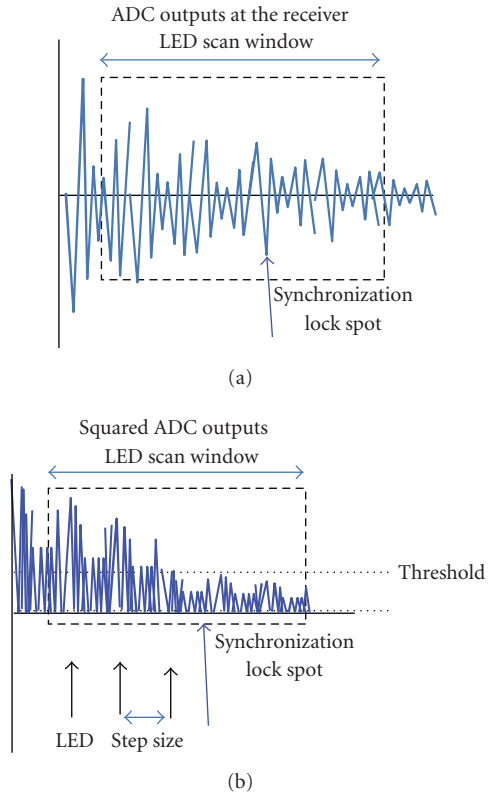

Figure 3: LED detection. (a) shows ADC outputs at the receiver contained in the payload segment. (b) shows squared values and scan window. The scan window is searched for the earliest received energy relative to the synchronization lock point. Scan window size and step size are user specified.

several processing steps, and then returns the range response packet at time stamp ts_3. The response packet contains the time delay on the responding radio, $\Delta t_{32} = ts_3 - ts_2$. The requester time stamps the arrival of the response packet, ts_4. From Figure 2, letting $\Delta t_{41} = ts_4 - ts_1$ the coarse measurement of propagation delay, τ' is given by

$$\tau' = \frac{\Delta t_{41} - \Delta t_{32}}{2}. \tag{3}$$

The coarse time stamps ts_4 and ts_2 are taken when the correlators achieve acquisition. Depending on the channel response, this may not be the leading edge of the pulse.

Instead of conventional data, the payload of range packet contains the received analog-to-digital conversion (ADC) outputs. This information is used to refine the coarse measurements for ts_2 and ts_4 using an LED algorithm supplied by the user. Currently, our LED algorithm simply squares the ADC output and scans for the earliest amount of energy that crosses a specified threshold relative to the synchronization lock spot, as shown in Figure 3. The LED algorithm parameters include LED scan window size and scan step size. The scan window size determines the time interval, relative to the lock point, that ADC outputs are captured. The scan step size determines the sampling interval used when searching for the leading edge. A large scan window and small scan step size provides increased accuracy and robustness for LED, especially in a dense multipath environment. However, both settings also affect the time required to complete a ranging operation. As a figure of merit, the transmission delay for the preamble with automatic thresholding and synchronization integration = 64 is determined from (2) as $64 \times 443/9.6 \times 10^6 \times 1.5 \approx 4.43$ milliseconds. A scan window setting of = 20 nanoseconds and scan step size = 54 ps leads to a 3.2 milliseconds delay for LED. Practical values for a single range measurement range from 10 milliseconds to 30 milliseconds depending on the various parameter settings. Different settings offer a tradeoff between better performance against increased delay. Once the parameters are specified, the packet transmission time is fixed.

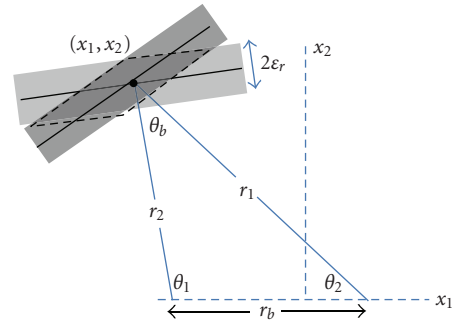

Figure 4: Parallelogram defined by range error ε_r and angle θ_b represents the magnitude of the position error.

2.3. Position Measurements. The radios on the vehicle represent coordinate nodes that obtain the range to the operator and send range measurement and status information to the controller. The controller monitors and controls the system and also collects range data and determines positions. The coordinate radios and controller share information using UDP/IP packets over Ethernet. Mean UDP packet delay was measured at 270 microseconds with a variance of 40 microseconds. Since range delays are on the order of 10^{-2} s, the UDP packet delays are not a primary consideration.

To analyze position error in two coordinates, let $\{\varepsilon_r\}$ represent the distribution of range errors and let each range measurement have a random error denoted by $\varepsilon_{r,i} \in \{\varepsilon_r\}$. The resulting position error can be analyzed by examining the area created by the intersection of two measured ranges, $r_1 + \varepsilon_{r,1}$, and $r_2 + \varepsilon_{r,2}$ as shown in Figure 4. For simplification, we approximate the arcs representing the

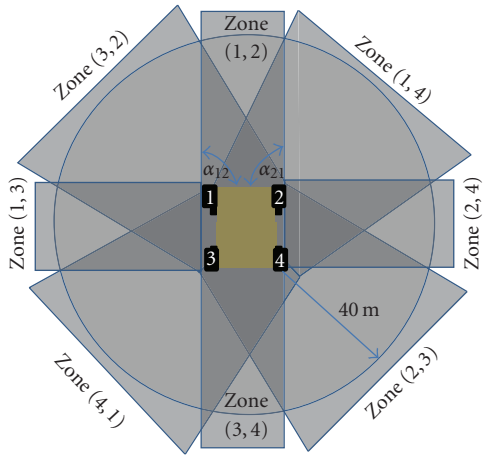

Figure 5: Eight zone definitions defined by coordinate radio pairs. Ambiguous positions resulting from bilateration will never be in the same zone.

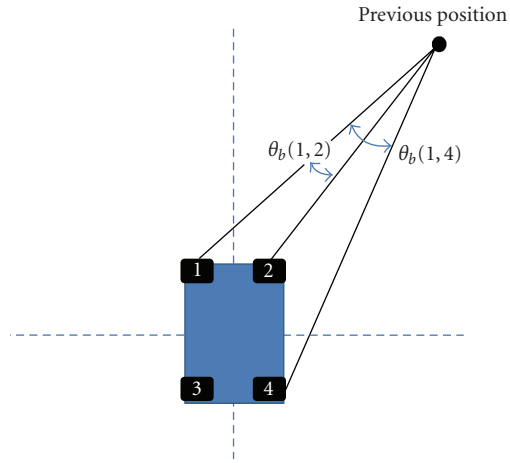

Figure 6: Minimizing GDOP per radio pair selection. The largest angle $\theta_b(i, j)$ from the last position measurement indicates the smallest GDOP based on (4). This is used to determine which two radios are used for the next position measurement. In this case radio pairs (1,4) yield the lowest GDOP.

intersection of range measurements as straight lines. Then the parallelogram created by intersection of two measured ranges represents the distribution of the position error. It can be shown that the area of the parallelogram is given by

$$\left(\frac{\varepsilon_{r1}\varepsilon_{r2}}{\sin\theta_b}\right), \tag{4}$$

and that this area and hence position error decrease as θ_b increases from $0^\circ < \theta_b \leq 90^\circ$ and it is minimized when $\theta_b = 90^\circ$. Decreasing either the separation distance between the target platform or $|\theta_1 - \theta_2|$ will cause θ_b to increase. The increased position error due to decreasing θ_b is known as geometric dilution of precision (GDOP) and has been well studied [16].

In this system, the four coordinate nodes are spaced so as to limit GDOP and eight zones are defined using radio pairings as shown in Figure 5 to balance the affects of GDOP between zones. Zone boundaries are defined by the angles α_{ij} relative to the coordinate radio locations. We define the angles α_{ij}, such that the worst case (smallest) θ_b along any two bordering zones IS equal which balances the affect of DOP between zones and limits the affect of DOP in any one zone. At each update, the controller selects a pair of coordinate radios to range to a target that minimizes GDOP. For example, let $\theta_b(i, j)$ be the angle defined by range measurements r_i and r_j taken from radios i and j to the target's last measured position. Consider the situation in Figure 6, we compute $\theta_b(1,4)$ and $\theta_b(1,2)$ for radio pairs $(1,4)$ and $(1,2)$. By inspection $\theta_b(1,4) > \theta_b(1,2)$, thus $(\varepsilon_{r1}\varepsilon_{r2}/\sin\theta_b(1,4)) < (\varepsilon_{r1}\varepsilon_{r2}/\sin\theta_b(1,2))$, and the GDOP will be smaller for radio pairs $(1,4)$.

Factors, such as primary direction of travel and safety restrictions, can be used to further refine zone boundaries. DOP is well studied [18] and detailed discussion of DOP and zone coverage is not provided in this paper.

Normally, trilateration is required to eliminate an ambiguous position (x_1', x_2') shown in Figure 7. However, the valid position between these two possibilities can be

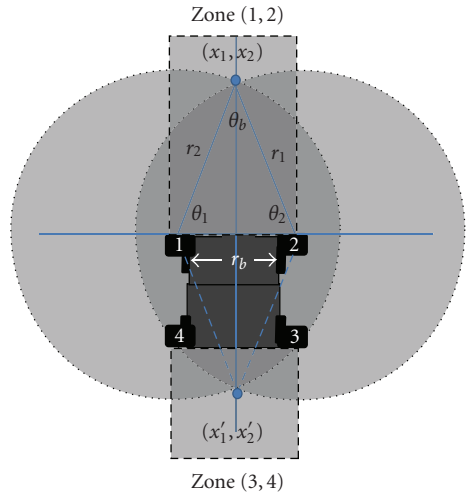

Figure 7: Bilateration for position measurement in a plane. Ambiguous position at (x_1', x_2') is eliminated by assigning targets into zones based on last measurement.

determined by using zones in such a way that GDOP is kept small and the history of the target's zone locations IS recorded. For example, in Figure 7, the locations (x_1, x_2) and (x_1', x_2') are discernable because they are located in different zones. This allows us to measure position using only two range measurements which reduces the time to measure position by an average of 33%. From Figure 6, bilateration is used to determine a position, (x_1, x_2), from two ranges, r_1 and r_2 as

$$\theta_2 = \cos^{-1}\left(\frac{r_1^2 + r_b^2 - r_2^2}{2r_1 r_b}\right), \tag{5}$$

where the position in two coordinates is defined by $(x, y) = r_1 \angle \theta_2$. If ambiguity is introduced because of position measurement errors and then historical position data or

a third range is used to determine the correct measured position. If a range packet is dropped or detected to have a large error (outlier), then additional ranges can be requested. In practice, the number of retries is limited by an algorithm that looks at the delay impact to the target update rate for all other targets.

2.4. MAC and Tracking Multiple Targets. Media access control (MAC) is required to coordinate range packets between various radios. Since the system is inherently centralized about the platform, we opt for a centrally controlled, polling MAC that resides on the controller and uses polling time slots to track each target. The controller uses past position measurements to determine which coordinate radios and target will be involved in the next polling event. In the initial phase, polling is round robin between targets. Processing time for various filters and bounds checking is less than 1 milliseconds. If we assume 5 targets with two range measurements for each position and a delay of 20 milliseconds per range, then the system will have an overall update rate of approximately 5 Hz per target.

3. Experimental Data Collection and Analysis of Static Position Measurements

An experiment was conducted to establish a baseline assessment of performance limitations for range accuracy under the simplified conditions of an unobstructed channel on level terrain during the initial development of the system. Range data was collected in an open grassy field and in an urban environment at distances from 2 m to 42 m in 2 m increments. The heights of the transmit antennae, h_{tx}, and receive antenna, h_{rx}, were both set to 1 m. Truth points were established using a high precision laser with a mean accuracy of 0.002 m and a variance of 0.001 m. At each truth point, 4000 range samples were collected and the individual range measurements, number of dropped range packets, outliers, and successful range measurements were recorded.

Generally, the attempt to measure a range can have one of three results: a dropped range packet, a large range error, also called an *outlier*, or a successful range attempt. A dropped range packet occurs when synchronization is not achieved over the preamble and the range attempt fails. This occurs when the received SNR is insufficient, either due to path loss or fading. A large range error can be caused by fading or by a system problem, such as the scan window being too small relative to channel delay spread. Typically outliers have a measurement differential from the preceding range in excess of several meters. In our static data collection, we set a threshold of 1 meter for outliers. A successful range attempt will have some small error associated with fading or uncertainty in leading edge detection (LED).

Preliminary experiments were conducted to evaluate a wide range of parameter settings. Parameters were selected that balanced accuracy of range measurements against time duration to complete a ranging operation. Automatic synchronization thresholding was selected, as experiments verified that it is not possible to reliably cover distances from 2 m to 42 m using a static threshold. Experiments with correlator step size show significant increase in packet loss with step sizes greater than the default 235 ps. The synchronization integration was selected in order to minimize the effects of path loss at a maximum range of 40 m. The synchronization parameters for integration and step size were set to 64 and 235 ps, respectively. The received symbol must have enough energy, E_s^{rx}, to overcome path loss effects at $d = 40$ m. For analysis of path loss in a LOS channel over flat ground with $d \gg \sqrt{h_{tx}h_{rx}}$, we assume that power falls off at 40 dB/decade [19]. Thus at $d = 40$ m, we would expect pathloss, $L_p \approx -96$ dB. The average transmitted power of a pulse over the frequency range from 3.1 GHz to 5.8 GHz is given as

$$P_{TX} = 32\,\mu\text{W}. \tag{6}$$

If synchronization integration is set to 64, this yields transmitted symbol energy of

$$E_s^{tx} = -66.71\,\text{dBm} \cdot \text{s}. \tag{7}$$

If Noise power spectral density is assumed to be $N_0 = -174\,\text{dBm}\cdot\text{s}$, then received symbol energy to power spectral density is given:

$$\begin{aligned}\frac{E_s^{rx}}{N_0} &\approx -66.71\,\text{dBm} \cdot \text{s} + 174\,\text{dBm} \cdot \text{s} - 96\,\text{dB} \\ &= 11.29\,\text{dBm} \cdot \text{s}.\end{aligned} \tag{8}$$

The radios use BPSK modulation, hence the symbol error rate, P_e, is given as

$$P_e = Q\left(\sqrt{\frac{2E_s}{N_0}}\right) \approx 10^{-6}. \tag{9}$$

For a preamble length $n = 443$ symbols, and if $n \cdot Pe \ll 1$, then the probability of dropping a packet is given by

$$P_f \approx n \cdot \ P_e \approx 0.4\% \tag{10}$$

(see [20]). Thus if synchronization integration is set to 64, path loss should not be a significant factor in packet loss rate. Experimental data shows that there is no significant correlation between distance and dropped packets and we conclude that dropped packets in an open channel at distances from 2 m to 40 m are primarily the result of fading.

The leading edge detection parameter for scan step size was set to $\tau_{\text{step}} = 54$ ps or 0.162 cm which is about 23% of a pulse width. If a sample misses the leading edge on average by $\tau_{\text{step}}/2$, then we would expect a mean bias of 0.08 cm for each of the LED operations, for a total mean bias of 0.162 cm. Multipath components can obscure the leading edge also contributing to range errors. Measurements revealed a mean round trip bias of 0.18 cm using these settings. The scan window size was evaluated at two values, 20 nanoseconds and 100 nanoseconds. Preliminary experiments showed that 20 nanoseconds is the minimal size that offers reliable performance in a wide range of conditions and has a delay of approximately 3.2 milliseconds for LED with $\tau_{\text{step}} = 54$ ps.

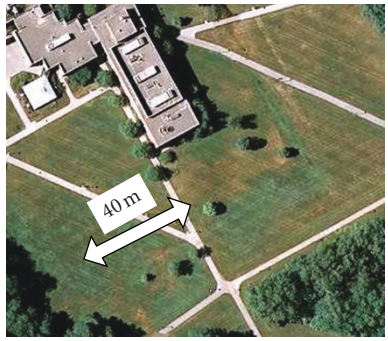

(a)

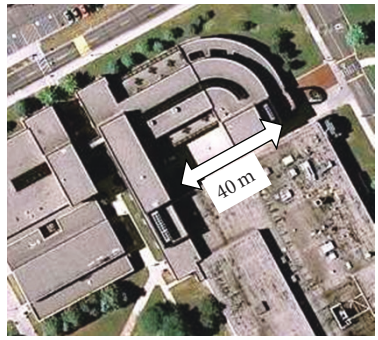

(b)

Figure 8: Top view of open channel right and urban channel left.

The 100 nanoseconds window size was selected for the urban environment, where delay spread can be a very significant factor. The delay measured for the 100 nanoseconds window with $\tau_{\text{step}} = 54$ ps is 6.7 milliseconds. The total constant delay for range measurements at 20 nanoseconds and 100 nanoseconds scan window is 20.01 milliseconds and 27.10 milliseconds, respectively. Assuming a successful range measurement, we expect range measurement errors to result primarily from LED sampling error and multipath fading. Experiments verify that the mean and variance of range errors are not correlated with distance.

The open channel is in a 40 m grassy area with some trees and buildings at distances greater than 30 m on either side of the channel. There are several small trees within 20 m of the channel. The urban channel is enclosed on three sides with four to five story buildings. The fourth side is partially obstructed by a 3-story building and has a narrow driveway extending for 25 m with 2- and 3-story buildings on either side. Figure 8 shows a top view of the open and urban channel on the right and left respectively.

In Figure 9, the round markers graph shows the distribution of experimental range errors for open channel and urban channel with 20 nanoseconds and 100 nanoseconds scan window, adjusted for LED bias as described in the previous section. Figures 9(a) and 9(b) show the open and urban channels for 20 nanoseconds scan window and Figures 9(c) and 9(d) show the open and urban channels for the 100 nanoseconds scan window, respectively. It can be seen that the measured range errors closely follow a Gaussian distribution. A theoretical distribution was developed by determining the minimum mean squared error iteratively for the mean and standard deviation for each data set. The model for each of the four cases is shown in Figure 8 as the solid line. Table 2 shows mean and standard deviation for range error for open and urban channel with 20 nanoseconds and 100 nanoseconds scan window for the measured data and model. The measured and theoretical means are zero-mean when considering that the laser used to measure truth has a 0.002 m mean error. The measured data is slightly asymmetrical about the mean with a standard deviation of approximately 2 cm for the open channel. The standard deviation for the urban channel is significantly larger at 3.8 cm and 3.0 cm for the 20 nanoseconds and 100 nanoseconds window, respectively. The smaller standard deviation of the for the 100 nanoseconds window size suggests an accuracy advantage in urban channels for the 100 nanoseconds window size. The data for the model has a slightly smaller standard deviation and is symmetrical about the mean.

Table 2: Mean and standard deviation (m) for range errors for measured and theoretical model for open and urban channel and scan window = 20 nanoseconds and 100 nanoseconds.

Range error, mean and standard deviation (m)				
Channel type	Open		Urban	
Scan window (ns)	20	100	20	100
Measured mean	0.002	−0.004	0.009	0.003
Theoretical mean	0.002	0.001	0.002	0.001
Measured Std Dev	0.020	0.024	0.038	0.030
Theoretical Std Dev	0.018	0.020	0.023	0.021

Table 3: % Outliers, % dropped packets, and total lost ranges for open and urban channel with 20 nanoseconds and 100 nanoseconds scan window.

Channel type	Open		Urban	
Scan window (ns)	20	100	20	100
% Range outliers	0.1	0.01	8	1.6
% Dropped packets	7	8	26	27
% Lost ranges	7.1	8.01	34	28.6

Table 3 provides the percentage of dropped and outlier packets. In the open channel there are almost no outliers for either setting and both have similar percentage of dropped packets for the 20 nanoseconds and 100 nanoseconds scan windows. This indicates that multipath fading is not a significant issue in an open channel and that a smaller scan window is more effective because of the lower delay per range measurement. The percentages of lost packets do not show correlation to distance in the open channel; thus we assume that the packet loss rate of 7% to 8% for the open channel is due to multipath effects from the grassy surface and buildings and trees that are near the channel. In the urban channel, outliers are 8% and 1.6% for the 20 nanoseconds and 100 nanoseconds scan windows, respectively. This shows the advantage of the larger scan window in a dense multipath environment. However, in the urban channel, the percentage of dropped

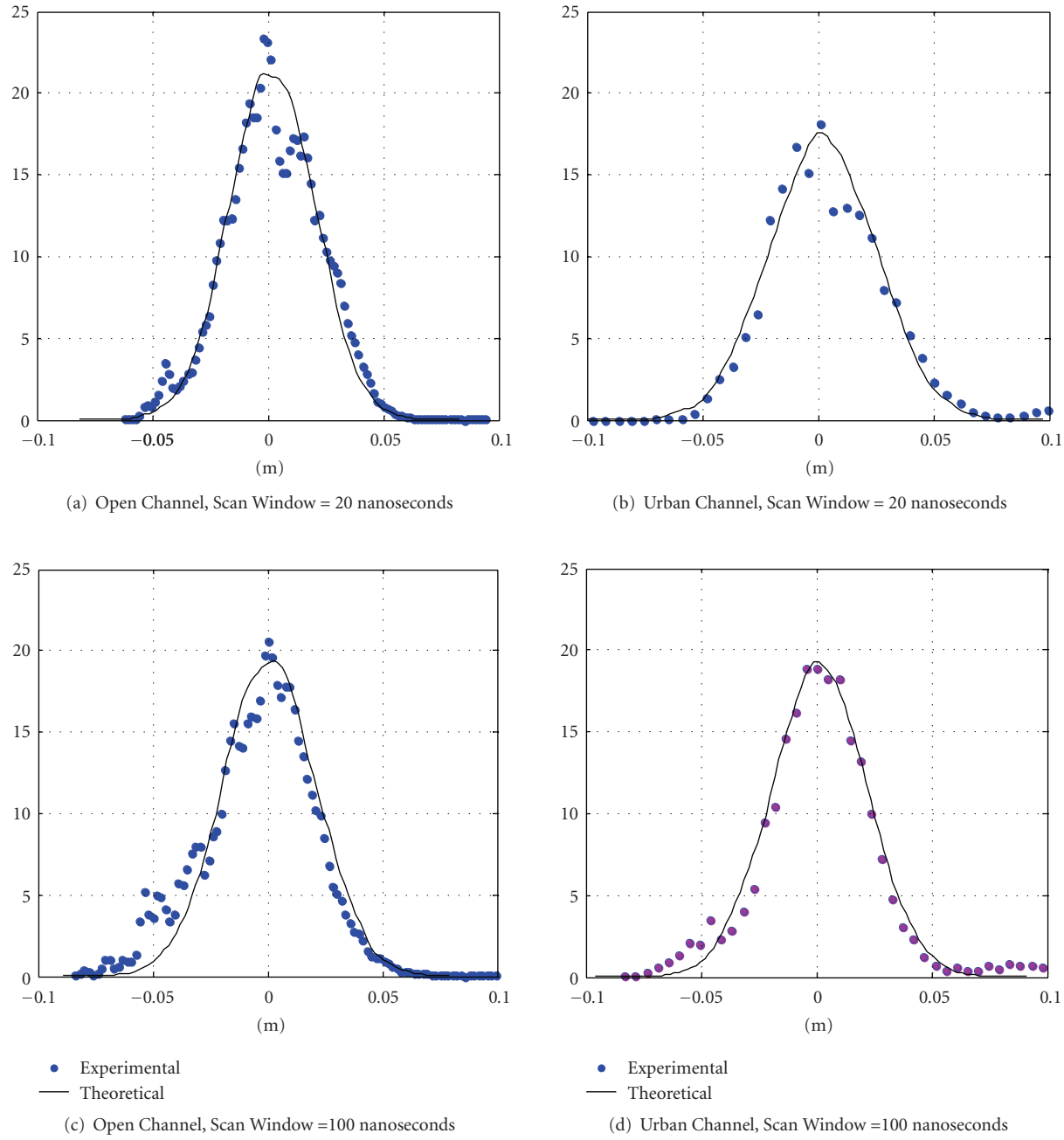

(a) Open Channel, Scan Window = 20 nanoseconds

(b) Urban Channel, Scan Window = 20 nanoseconds

(c) Open Channel, Scan Window =100 nanoseconds

(d) Urban Channel, Scan Window =100 nanoseconds

Figure 9: Distribution of range errors for (a) open channel, 20 nanoseconds scan window, (b) urban channel 20 nanosecond scan window, (c) open channel with 100 nanosecond scan window, and (d) urban channel with 100 nanoseconds.

packets dominates the total lost ranges and both settings have similar percentage of dropped packets. This indicates that dropped packets due to multipath fading are a more significant impediment than outliers in urban channels.

3.1. Position Error in a Static Environment. From two ranges, r_1 and r_2, we can determine the angle θ_2 and position given by $r_1 \angle \theta_2$, as described in Section 2. Let $\{\varepsilon_r\}$ represent the range error distribution and $\varepsilon_{r,i} \in \{\varepsilon_r\}$ a sample from the distribution. Then the error in the angle θ_2 can be represented as

$$\varepsilon_{\theta 2} = \cos^{-1}\left(\frac{(r_1+\varepsilon_{r,1})^2 + r_b^2 - (r_2+\varepsilon_{r,2})^2}{2r_b(r_1+\varepsilon_{r,1})}\right) - \cos^{-1}\left(\frac{r_1^2+r_b^2-r_2^2}{2r_1r_b}\right). \tag{11}$$

Then the measured position is given as

$$\hat{r}_1 \angle \hat{\theta}_2 = (r_1+\varepsilon_{r,1}) \angle (\theta_2 + \varepsilon_{\theta 2}). \tag{12}$$

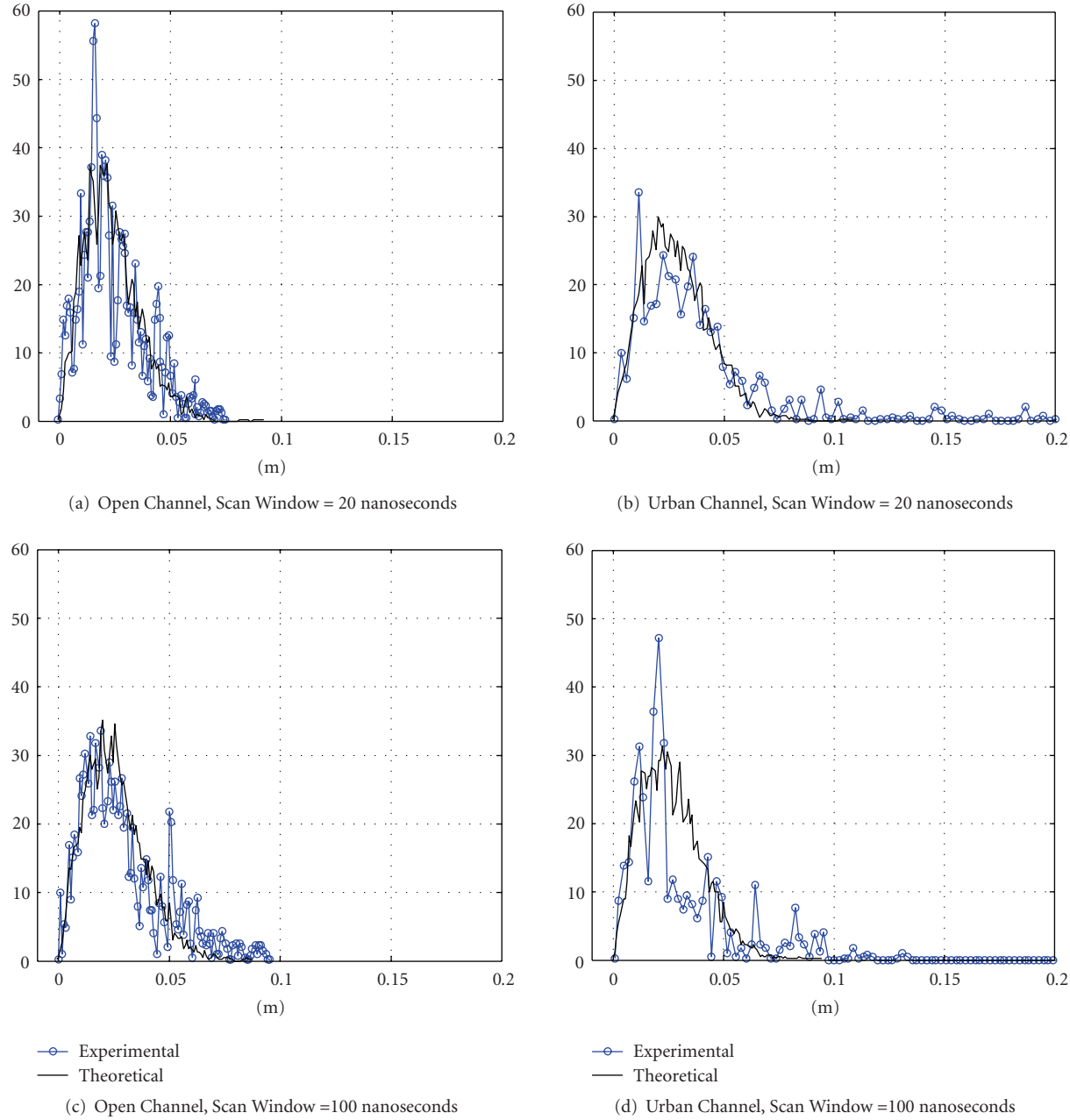

(a) Open Channel, Scan Window = 20 nanoseconds

(b) Urban Channel, Scan Window = 20 nanoseconds

(c) Open Channel, Scan Window =100 nanoseconds

(d) Urban Channel, Scan Window =100 nanoseconds

FIGURE 10: The distribution of static position errors for 20 nanoseconds scan window in (a) open and (b) urban channel and for 100 nanoseconds scan window in (c) open and (d) urban channel, for $\theta_b = 90^\circ$ and $\theta_1 = 45^\circ$.

For two coordinates, x_1 and x_2 with measured values $(\hat{x}_1, \hat{x}_2) = f(\hat{r}_1 \hat{r}_2)$, we can determine the error in position measurement as

$$\begin{bmatrix} \varphi_1 \\ \varphi_2 \end{bmatrix} = \begin{bmatrix} x_1 - \hat{x}_1 \\ x_2 - \hat{x}_2 \end{bmatrix}. \tag{13}$$

Letting μ_{φ_i}represent the mean value of ϕ_i, the RMS of the position error at time is given by

$$\varphi_{\text{RMS}} = \sqrt{\mu_{\varphi_1}^2 + \mu_{\varphi_2}^2}. \tag{14}$$

Note that geometric effects will cause $\varphi_i(k)$ to grow as range and angle between the target and platform increase. The distribution of position errors is determined for the case when $\theta_b = 90^\circ$ and $\theta_1 = 45^\circ$, which minimizes geometric errors and allows us to focus on position errors due to range errors. Figure 10 shows the distribution of magnitude of the position errors for experimental and theoretical range errors. Figures 10(a) and 10(b) shows the case for open and urban channel with 20 nanoseconds scan window and Figures 10(c) and 10(d) show the case for open and urban channel with 100 nanoseconds scan window. The increased variance in position error due to dense multipath for the urban channel is evident for both radio settings. The position error generated by using the model for range error follows the distribution of the measured position errors, indicating

Table 4: Mean update delay for open and urban channel with 20 nanoseconds and 100 nanoseconds scan window.

Channel type	Open		Urban	
Scan window (ns)	20	100	20	100
Mean update delay (ms)	43.23	59.29	54.81	71.31
Std Dev update delay (ms)	48.59	92.41	113.76	192.76

that a model using Gaussian range errors can provide reasonable results for analyzing position error in open and urban channels.

Table 4 shows the mean and standard deviation for position update delay, which includes the effects of dropped packets, outliers, and invalid position measurement. The later occurs when range errors and geometry result in a non-real solution to position (e.g., θ_1 is complex). For the open channel, less than 10% of position measurements needed more than two range measurement attempts wherease in the urban case, as many as 34% of position measurements needed more than two range attempts. The penalty for the additional delay for the larger scan window is clear when examining the mean position update delay for both scan window sizes. For the open and urban channel, the 100 nanoseconds window size has a mean position update delay that is approximately 27% larger than the 20 nanoseconds case. In the next section the impact of this additional delay will be examined in a mobile environment.

4. Mobility Model and Total Measurement Error

In this section we analyze position accuracy for a target in motion based on the experimental data collection. For a mobile target, additional uncertainty in the position measurement is generated due to the finite duration of the range measurements and the interval between position updates. We propose a mobility model based on platform specifications and determine the resulting errors in position measurement due to mobility.

4.1. Mobility Model. The mobility model aims at examining position error in the worst case situations where the operator and platform are approaching each other with a mean relative velocity equal to the maximum allowable relative velocities specified in Table 1. Flat terrain is assumed and position is measured in two coordinates. A random, zero-mean, piecewise constant acceleration is applied in both coordinate directions with a standard deviation of 1 m/s^2. The relative distance between the platform and operator varies from 3 m to 40 m. A total of five crew members are tracked so that the update of the each position is delayed by four additional position measurements. Recall that each pair of coordinate radios is assigned a zone in such a way that errors due to geometry are balanced between zones. Because of this, analysis is restricted to motion in front of the vehicle and we assume that motion is confined to $\alpha_{11} < 90^\circ$ and $\alpha_{12} < 90^\circ$, shown in Figure 5.

The position update rate $T(k)$ at any time k varies randomly, depending on the occurrence of dropped range packets. Let Δ_k represent the time of the kth position update, where $\Delta k = \sum_{i=1}^{k-1} T(i)$. If we assume that random acceleration is piecewise constant between the sampling intervals $\Delta_k < t < \Delta_{k+1}$ then the position of the target at time t in each coordinate is described by

$$x_i(t) = x_i(t_0) + t\bar{\dot{x}}_i(t), \tag{15}$$

where $t_0 = \Delta_k$ and $\bar{\dot{x}}_i(t)$ is the mean velocity over the interval $\Delta_k < t < \Delta_{k+1}$.

Since $\bar{\dot{x}}_i(t) = (\dot{x}_i(t_0) + \dot{x}_i(t))/2$, $\dot{x}_i(t) = \dot{x}_i(t_0) + t\bar{\ddot{x}}_i(t)$, and $\bar{\dot{x}}_i(t) = \dot{x}_i(t_0) + t\bar{\ddot{x}}_i(t)/2$, we have

$$x_i(t) = x_i(t_0) + t\dot{x}_i(t_0) + \frac{t^2\bar{\ddot{x}}_i(t)}{2}. \tag{16}$$

As $\ddot{x}_i(t)$ is constant during the interval from Δ_k to Δ_{k+1}, then $\bar{\ddot{x}}_i(t) = \ddot{x}_i(t_0)$ and for $\Delta_k < t < \Delta_{k+1}$ we have the position and velocity given by

$$\begin{aligned} \dot{x}_i(t) &= \dot{x}_i(t_0) + t\ddot{x}_i(t_0), \\ x_i(t) &= x_i(t_0) + t\dot{x}_i(t_0) + \frac{t^2\ddot{x}_i(t_0)}{2}. \end{aligned} \tag{17}$$

For a position measurement that occurs at $\Delta_k = t_0$ the true position for each dimension is given by

$$x_i(k) = x_i(k-1) + T(k-1)\dot{x}_i(k-1) + \frac{T(k-1)^2\ddot{x}_i(k-1)}{2}. \tag{18}$$

The mobility model for the discrete two dimensional case is given by

$$\begin{aligned} \begin{bmatrix} x_1(k+1) \\ \dot{x}_1(k+1) \\ x_2(k+1) \\ \dot{x}_2(k+1) \end{bmatrix} &= \begin{bmatrix} 1 & T(k) & 0 & 0 \\ 0 & 1 & 0 & 0 \\ 0 & 0 & 1 & T(k) \\ 0 & 0 & 0 & 1 \end{bmatrix} \begin{bmatrix} x_1(k) \\ \dot{x}_1(k) \\ x_2(k) \\ \dot{x}_2(k) \end{bmatrix} \\ &\quad + \begin{bmatrix} \frac{1}{2}T(k)^2 & 0 \\ T(k) & 0 \\ 0 & \frac{1}{2}T(k)^2 \\ 0 & T(k) \end{bmatrix} \begin{bmatrix} \ddot{x}_1(k) \\ \ddot{x}_2(k) \end{bmatrix}, \end{aligned} \tag{19}$$

where $x_1(k)$ and $x_2(k)$ are position measurements for each dimension and $\ddot{x}_1(k)$ and $\ddot{x}_2(k)$ are assumed to be zero mean random processes that are treated as process noise. Table 5 shows the initial values for each state. In a manner similar to the static case (13) and (14), the error and RMS error in measured position at the kth measurement is given by

$$\begin{aligned} \begin{bmatrix} \varphi_1(k) \\ \varphi_2(k) \end{bmatrix} &= \begin{bmatrix} x_1(k) - \hat{x}_1(k) \\ x_2(k) - \hat{x}_2(k) \end{bmatrix}, \\ \varphi_{\text{RMS}} &= \sqrt{\mu_{\varphi_1}^2 + \mu_{\varphi_2}^2}. \end{aligned} \tag{20}$$

Table 5: Initial values for mobility model for four test cases.

Initial state	Case 1	Case 2	Case 3	Case 4
$x_1(0)$	0 m	0 m	0 m	0 m
$\dot{x}_1(0)$	0 m/s	0 m/s	0 m/s	0 m/s
$x_2(0)$	3 m	3 m	3 m	3 m
$\dot{x}_2(0)$	1.1 m/s	2.2 m/s	3.3 m/s	4.4 m/s

Table 6: Delays during the range measurement that cause additional range measurement uncertainty for 20 nanoseconds and 100 nanoseconds scan windows in a mobile channel.

Scan window size	τ	$\tau/2$	$3\tau/2$
20 ns	20.01	10.05	30.15
100 ns	27	13.50	40.05

Target motion during the range measurement process tends to increase the uncertainty of range measurements. If round trip range delay is given as τ, the request and reply take approximately $\tau/2$ to complete. The processing for position determination and managing the UWB system has a mean delay of 400 microseconds. Target motion during a range packet's time of flight is much less than 1 microsecond for the ranges under consideration. Since τ has a magnitude of 10^{-2} seconds, both of these later factors are insignificant and are ignored. The error due to target motion is initialized upon receipt of the range request packet at the target. Assuming that range measurement attempts are successful, the delay between receipt of the first range request and the completion of the position measurement is approximated as $3\tau/2$. The delay between the receipt of the second range request and completion of the position measurement is approximated as $\tau/2$. The additional delays are incorporated into the simulation model and will affect range and position measurement errors, depending on the relative mobility characteristics between the target and the platform. The delays for each scan window size are shown in Table 6.

Given a continuously moving target, the position error at any time, t, will be affected by the interval between position measurements. The position update interval depends on the time taken to measure range, the total number of range attempts needed to determine a position, and the number of targets being tracked. In our system, at least two range attempts are required, possibly more in the event of dropped range packets or outliers. If we assume that targets are updated in a round robin manner, then we have $T_j(k)$ the position update date delay for the kth position for the jth target as

$$T_j(k) = \sum_{i \neq j}^{N} \tau n_i(k), \tag{21}$$

where τ is the constant time to complete a range measurement for a given radio setting; $n_i(k)$ is the total number of ranges measurements for the ith target on the kth iteration; N is the total number of targets, assumed to be constant.

From (15) we are given $x(t)$ the position of the target at any time t. If the most recent measured position is given by $[\hat{x}_1(k), \hat{x}_2(k)]$, then at some time t_0, where $\Delta_k < t < \Delta_{k+1}$, the error between the true position $[x_1(t_0), x_2(t_0)]$ and the last measured position $[\hat{x}_1(k), \hat{x}_2(k)]$ is given by

$$\begin{bmatrix} \phi_1(t_0) \\ \phi_2(t_0) \end{bmatrix} = \begin{bmatrix} x_1(t_0) - \hat{x}_1(k) \\ x_2(t_0) - \hat{x}_2(k) \end{bmatrix}. \tag{22}$$

Letting μ_{ϕ_i}represent the mean value of ϕ_i, the RMS of the total error at time is given by

$$\phi_{\text{RMS}} = \sqrt{\mu_{\phi_1}^2 + \mu_{\phi_2}^2}. \tag{23}$$

Note that at $t_0 = k$, $\varphi_i(k) = \phi_i(t_0)$.

4.2. Simulation. Figure 11 shows φ_{RMS} over distances from 3 m to 40 m as mean relative velocity increases from 1.1 m/s to 4.4 m/s. Figures 11(a) and 11(b) show the case for open channels for the 20 nanoseconds and 100 nanoseconds scan window, respectively. Figures 11(c) and 11(d) show the case for the urban channels for the 20 nanoseconds and 100 nanoseconds scan window, respectively. Effects of GDOP can be seen as φ_{RMS} grows with increasing separation distance from 3 m to 40 m. In the urban channel φ_{RMS} at given distances is higher than for the open case when comparing scan windows of the same size. This is due to the increased variation in range errors caused by the dense multipath in the urban channel. Notably, φ_{RMS} for the 100 nanoseconds case is significantly larger due to the additional delay experienced during range measurements as the target continues to move. This effect amplifies as mean relative velocity increases from 1.1 m/s to 4.4 m/s, resulting in divergence of the graphs as velocity increases. The trend is similar for both the urban and open channel cases. This indicates that the interrange time delay is the dominant factor for φ_{RMS} in a mobile channel.

Figure 11 shows ϕ_{RMS} over distances from 3 m to 40 m. Figures 12(a) and 12(b) show the case for open channels using 20 nanoseconds and 100 nanoseconds scan window, respectively. Figures 12(c) and 12(d) show the case for the urban channels using 20 nanoseconds and 100 nanoseconds scan window, respectively. Initially the error between updates, described by (23) is dominant, resulting in the saw tooth pattern, created as $\phi_i(t)$ grows between position updates, then drops when $\phi_i(t) = \phi_i(k)$ at the next position update. As with the previous figure, the impact of DOP can be clearly seen with increasing separation distance. The increasing error due to DOP and $\varphi(k)$ begins to obscures the saw tooth pattern caused by changes in $\phi_i(t)$. The ϕ_{RMS} is significantly more pronounced for the 100 nanoseconds scan window case for both open and urban channel, reflecting the combined effect of delay between range measurements and delays between position measurements. The effects of increasing velocity on these delays can be observed in the separation of individual graphs at different velocities.

5. Summary and Future Work

The most significant impact to position errors in the mobile channel includes affects caused by GDOP and errors caused

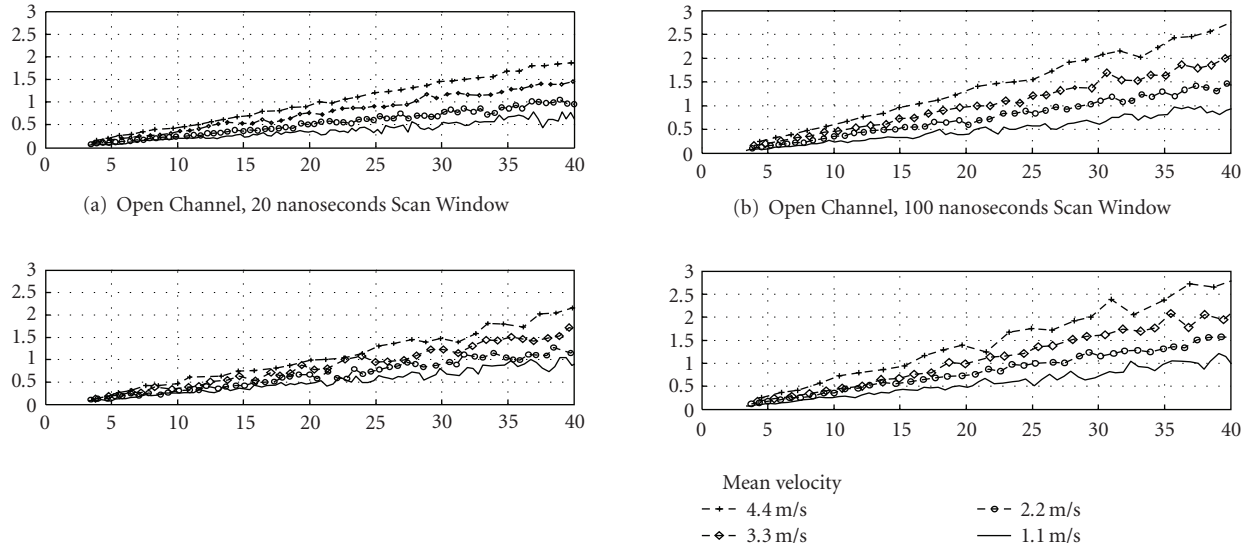

(a) Open Channel, 20 nanoseconds Scan Window

(b) Open Channel, 100 nanoseconds Scan Window

(c) Urban Channel, 20 nanoseconds Scan Window

(d) Urban Channel, 100 nanoseconds Scan Window

Figure 11: φ_{RMS} for distances ranging from 3 m to 40 m, for (a) 20 nanoseconds and (b) 100 nanoseconds scan window in an open channel and (c) 20 nanoseconds and (d) 100 nanoseconds in an urban channel with mean relative velocity ranging from 1.1 m/s to 4.4 m/s.

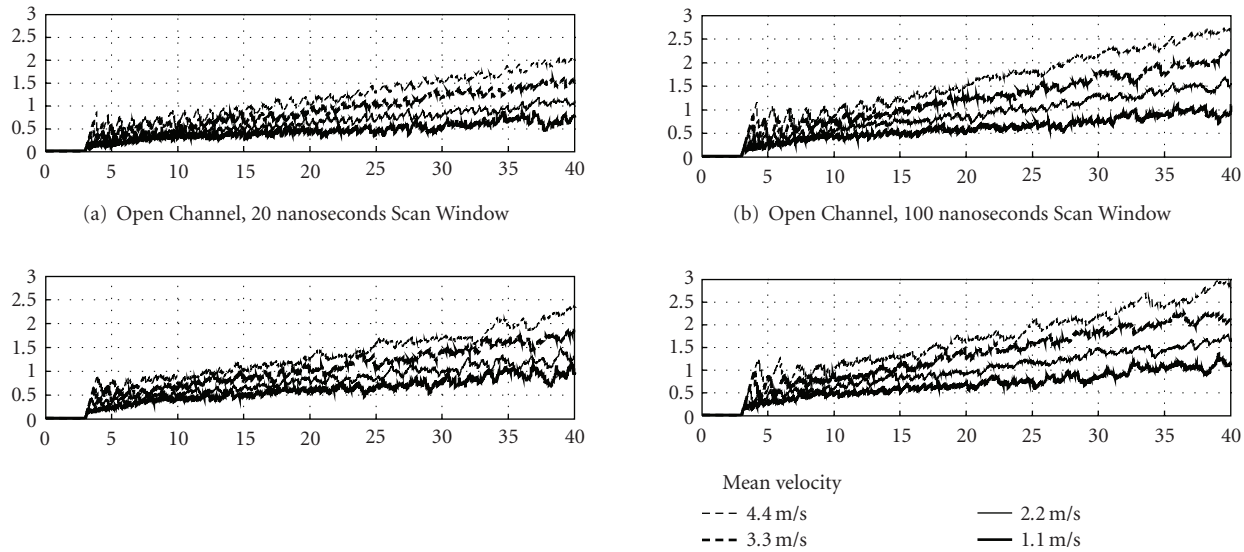

(a) Open Channel, 20 nanoseconds Scan Window

(b) Open Channel, 100 nanoseconds Scan Window

(c) Urban Channel, 20 nanoseconds Scan Window

(d) Urban Channel, 100 nanoseconds Scan Window

Figure 12: ϕ_{RMS} for distances ranging from 3 m to 40 m, for (a) 20 nanoseconds and (b)100 nanoseconds scan window in an open channel and (c) 20 nanoseconds and (d) 100 nanoseconds in an urban channel with mean relative velocity ranging from 1.1 m/s to 4.4 m/s.

by delay during ranging and position updates. Errors due to GDOP are limited by creating zones around the vehicles that balance GDOP between zones and attempt to maximize θ_b. Errors due to ranging and position update delays can be reduced by using the shorter 20 nanoseconds scan window option. This option is shown to be less effective than the 100 nanoseconds scan window in a dense multipath environment with respect to percentage of range outliers. However the problem with range outliers is seen to be relatively insignificant when compared to percentage of dropped packets and additional errors caused by the delays required for the larger scan window. The modeling strongly suggests that a smaller scan window that results in a shorter range measurement duration is more effective than a larger scan window, even in a dense multipath environment.

At closer distances (e.g., less than 10 m) and lower speeds (e.g., less than 2.2 m/s) where GDOP and delays are not as significant, the position accuracy is less than 0.5 m for 90% of cases using the 20 nanoseconds scan window. At greater distances and higher velocities, the combined effects of GDOP and delays cause position measurement errors result in mean errors exceeding 2.5 m for the 20 nanoseconds case

and 3 m for the 100 nanoseconds case. The primary concern for the positioning system is safety, and a recommendation has been made to alter the accuracy requirement to vary with distance and speed. Consider that platform's relative velocity is constrained based on distance from the operators for safety reasons. Using similar reasoning, we can have very stringent accuracy constraints when the platform is close to an operator, but these constrains can be relaxed as the platform get further away from the operators.

This effort presents the characterization of range and position error measurement results which serve as a foundation upon which this system can be matured and remaining challenges can be addressed. Currently, we are analyzing prediction and estimation capability that will yield improved accuracy over position measurements. An important consideration for development of an estimation technique includes the computational delay associated with a particular approach. Embedded systems tend to be power and cost constrained, limiting the amount of available processing resources. It will be important to contrast the performance of simple approaches with low computational overhead (e.g., variations of the alpha-beta filter) as well as more sophisticated approaches that yield more accurate estimates (e.g., particle filters) with realistic limitations on CPU performance. Another important aspect for this evolving capability is the study of more complex channel environments such as obstructed channels and transitions between different types of channels such as urban, forest, snow, and foliage.

Acknowledgment

This effort was supported by the Convoy Active Safety Technologies Program.

References

[1] J. Ni and R. Barton, "Design and performance analysis of a UWB tracking system for space applications," in *Proceedings of the IEEE/ACES International Conference on Wireless Communications and Applied Computational Electromagnetics*, pp. 31–34, April 2005.

[2] J. Ni, D. Arndt, P. Ngo, C. Phan, and J. Gross, "Ultra-wideband two-cluster tracking system design with angle of arrival algorithm," in *Proceedings of the IEEE National Radar Conference*, pp. 1–6, April 2006.

[3] V. Schwarz, A. Huber, and M. Tüchler, "Accuracy of a commercial UWB 3D location/tracking system and its impact on LT application scenarios," in *Proceedings of the IEEE International Conference on Ultra-Wideband (ICU '05)*, pp. 599–603, September 2005.

[4] H. Luediger, M. D. P. Guirao, D. Cassioli, and E. Stenzel, "Overview of an UWB system for LDR-L/T in industrial and logistics scenarios," in *Proceedings of the 16th IST Mobile and Wireless Communications Summit*, pp. 1–6, Budapest, Hungary, July 2007.

[5] T. H. Riehle, P. Lichter, and N. A. Giudice, "An indoor navigation system to support the visually impaired," in *Proceedings of the 30th Annual International Conference of the IEEE Engineering in Medicine and Biology Society (EMBS '08)*, pp. 4435–4438, August 2008.

[6] M. R. Mahfouz, C. Zhang, B. C. Merkl, M. J. Kuhn, and A. E. Fathy, "Investigation of high-accuracy indoor 3-D positioning using UWB technology," *IEEE Transactions on Microwave Theory and Techniques*, vol. 56, no. 6, pp. 1316–1330, 2008.

[7] O. Gremigni and D. Porcino, "Field trials of an accurate UWB ranging system," in *Proceedings of the IET Ultra Wideband Systems Seminar*, no. 11371, pp. 169–175, London, UK, April 2006.

[8] K. Yu and I. Oppermann, "Performance of UWB position estimation based on time-of-arrival measurements," in *Proceedings of the International Workshop on Ultra Wideband Systems*, pp. 400–404, May 2004.

[9] M. Navarro and M. Nájar, "TOA and DOA estimation for positioning and tracking in IR-UWB," in *Proceedings of the IEEE International Conference on Ultra-Wideband (ICUWB '07)*, pp. 574–579, Singapore, September 2007.

[10] R. Badorrey, Á. Hernandez, J. Chóliz, A. Valdovinos, and I. Alastruey, "Evaluation of TOA estimation algorithms in UWB receivers," in *Proceedings of the 14th European Wireless Conference (EW '08)*, pp. 1–6, Prague, Czech, June 2008.

[11] G. Zhang, S. Krishnan, F. Chin, and C. C. Ko, "UWB multicell indoor localization experiment system with adaptive TDOA combination," in *Proceedings of the 68th IEEE Vehicular Technology Conference*, pp. 1–5, Calgary, Canada, September 2008.

[12] J. Youssef, B. Denis, C. Godin, and S. Lesecq, "Enhanced UWB indoor tracking through NLOS TOA biases estimation," in *Proceedings of the IEEE Global Telecommunications Conference (GLOBECOM '08)*, pp. 1–5, November-December 2008.

[13] C.-D. Wann, Y.-J. Yeh, and C.-S. Hsueh, "Hybrid TDOA/AOA indoor positioning and tracking using extended Kalman filters," in *Proceedings of the 63rd IEEE Vehicular Technology Conference*, vol. 3, pp. 1058–1062, 2006.

[14] B. Denis, L. Ouvry, B. Uguen, and F. Tchoffo-Talom, "Advanced Bayesian filtering techniques for UWB tracking systems in indoor environments," in *Proceedings of the IEEE International Conference on Ultra-Wideband (ICU '05)*, pp. 6–10, September 2005.

[15] S. Venkatesh and R. M. Buehrer, "Non-line-of-sight identification in ultra-wideband systems based on received signal statistics," *IET Microwaves, Antennas and Propagation*, vol. 1, no. 6, pp. 1120–1130, 2007.

[16] J. A. Fernandez-Madrigal, E. Cruz-Martin, J. Gonzalez, C. Galindo, and J. L. Blanco, "Application of UWB and GPS technologies for vehicle localization in combined indoor-outdoor environments," in *Proceedings of the 9th International Symposium on Signal Processing and Its Applications (ISSPA '07)*, Sharjah, UAE, 2007.

[17] M. Tüchler, V. Schwarz, and A. Huber, "Location accuracy of an UWB localization system in a multi-path environment," in *Proceedings of the IEEE International Conference on Ultra-Wideband (ICU '05)*, pp. 414–419, Zürich, Switzerland, September 2005.

[18] P. Massatt and K. Rudnick, "Geometric formulas for dilution of precision calculations," *Journal of the Institute of Navigation*, vol. 37, no. 4, pp. 379–391, 1989.

[19] T. S. Rappaport, *Wireless Communications: Principles and Practice*, Prentice-Hall, Upper Saddle River, NJ, USA, 2nd edition, 2001.

[20] W. Stallings, *Data and Computer Communications*, Prentice-Hall, Upper Saddle River, NJ, USA, 8th edition, 2007.